Simultaneous Estimation of Super-resolved Depth and Image from Low Resolution Defocused Observations

Deepu Rajan
School of Biomedical Engg.
Indian Institute of Technology - Bombay
Mumbai, India 400 076
deepu@ee.iitb.ernet.in

Subhasis Chaudhuri
Dept. of Electrical Engg.
Indian Institute of Technology - Bombay
Mumbai, India 400 076
sc@ee.iitb.ernet.in

Abstract

This paper presents a novel technique to simultaneously estimate the depth and the focused image of a scene both at a super-resolution, from its defocused observations. Super-resolution refers to the generation of high resolution images from a sequence of low resolution images. Hitherto, the super-resolution technique has been restricted only to the intensity domain. In this paper, we extend the scope of super-resolution to acquire depth estimates at high resolution simultaneously. Given a sequence of low resolution, blurred and noisy observations of a static scene, the problem is to generate a dense depth map at a resolution higher than one that can be generated from the observations as well as to estimate the true focused image. Both the depth as well as the image are modeled as separate Markov Random Fields and a maximum a posteriori *method is used to derive a cost function which is then optimized using simulated annealing (SA).*

1 Introduction

Availability of high resolution images is often desirable in most computer vision applications. Be it remote sensing, medical imaging, robot vision, industrial inspection or video enhancement (to name a few), operating on high resolution images leads to a better analysis in the form of lesser misclassifications, better fault detection, more true-positives, etc. However, acquiring high resolution images is severely limited by the drawbacks of sensors that are cheaply available. Thus images acquired through such sensors suffer from aliasing and blurring. Aliasing occurs as a consequence of insufficient density of the detector array which causes frequencies above the Nyquist rate to alias, while blurring occurs due to integration of the sensor point spread function (PSF) at the sensor surface. An imaging sensor having a dense detector array is too expensive to be considered as an alternative to generate high resolution images. Hence, one must resort to image processing methods to construct a high resolution image from one or more available low resolution images. *Super-resolution* refers to the process of producing a high resolution image from several low resolution images. Many researchers have tackled the super-resolution problem both for still and video images [1, 2, 3, 4].

It was Pentland who first suggested that measuring the amount of blurring at a given point in the image could lead to computing the distance to the corresponding point in the scene, provided the parameters of the lens system are known [5]. This understanding ultimately led to extensive research in an area which came to be known as depth from defocus. Given two images of a scene recorded with different camera settings, we obtain two constraints on the spread parameters of the point spread functions corresponding to the two images. One of the constraints is obtained from the geometry of image formation while the other is obtained from the intensity formation in the defocused images. These two constraints are simultaneously solved to determine distances of objects in the scene.

In this paper, we expand the scope of super-resolution to include high resolution depth information in a scene, in addition to recovering intensity values. As mentioned earlier, one of the degradations in a low resolution image is the blur which produces a defocused image. We exploit this blur to generate a depth map through the depth from defocus formulation; moreover, now the depth map is estimated at a higher resolution than one that can be extracted from any of the observations. We call such a dense depth map as *super-resolved depth* obtained from defocused images. In addition to this, we also simultaneously estimate the true focused image of the scene.

In Section 2 and Section 3, we review the depth from defocus and the super-resolution techniques re-

spectively. We model the formation of the low resolution depth and image in Section 4 and describe the proposed method to simultaneously extract super-resolved depth and image in Section 5. Preliminary experimental results and conclusions are presented in Section 6 and Section 7, respectively.

2 Depth from Defocus

Recovery of 3-D information about a scene from its 2-D images has numerous applications such as robotic manipulation, automatic inspection, surveillance, etc. Over the years, a wide variety of techniques have been developed to extract structural information in a scene, e.g. depth from stereo, structure from motion, shape from shading and, more recently, depth from defocus (DFD).

The basic premise of depth from defocus is that since the degree of defocus is a function of lens setting and the depth of the scene, it is possible to recover the latter if the amount of blur can be estimated, provided the lens setting is known. An out-of-focus point light source images into a blurred circle [6], whose radius is described by a blur parameter σ defined as

$$\sigma = \rho \; r \; v \; (\frac{1}{f} - \frac{1}{v} - \frac{1}{u}), \tag{1}$$

where f is the focal length, u is the distance of the object point from the lens, v is the distance between the lens and the image detector, r is the radius of the lens aperture and ρ is a camera constant. Since the depth at various points in the scene may be varying continuously, σ would also vary all over the image. Given two defocused images of a scene with blur parameters σ_1 and σ_2, it can be shown that [7]

$$\sigma_1 = \alpha \; \sigma_2 + \beta \tag{2}$$

where α and β are constants that depend on the camera settings. The relative blur between the two defocused images estimated using the intensity information, together with equation (2), are used to solve for σ_1 and σ_2.

Early investigations of the DFD problem were carried out by Pentland [5] who measured the blur at known image characteristics like edges. In another method [6], he compared two images locally, one formed with a pin-hole aperture and then recovered the blur parameter through deconvolution in the frequency domain. In [7], Subbarao removed the constraint of one image being formed with a pin hole aperture by allowing several camera parameters like aperture, focal length and lens-to-image plane distance to vary simultaneously. The blur was recovered in the frequency domain through inverse filtering by assuming a local shift-invariance of the blur.

Recently, Chaudhuri and Rajagopalan have carried out a thorough investigation of the DFD prolem [8]. In [9], they use the complex spectrogram and the pseudo-Wigner distribution for recovering depth within the framework of space-frequency representation of the image. In [10], they extend this approach to impose smoothness constraints on the blur parameter and use a variational approach to recover depth. In [11], a MAP-MRF framework is used for recovering the depth as well as the focused image of a scene from two defocused images. However, the recovered depth map and image are at the same resolution as the observations. Other techniques for depth recovery and issues relating to optimal camera settings are described in [8].

In this paper, our aim is not only to recover depth from defocused images, but also to do so at a higher resolution. Thus given a sequence of low resolution blurred observtions of size $M \times N$, we wish to generate a dense depth map of size, say $qM \times qN$, where q is the upsampling factor. We call this the super-resolved depth estimate. Clearly, by doing this, we get a more accurate description of the depth in the scene, which eventually leads to a better performance of the task at hand.

3 Super-resolution Imaging

As indicated in the introduction, the physical limitations of currently available image sensors, such as size and density of detectors, impose a limit on the spatial resolution of images and videos. Also, the bandwidth limit set by the sampling rate also indirectly determines the resolution. These restrictions imposed by the sensor is sought to be removed by image processing methods, specifically by super-resolution restoration of images. The underlying philosophy of this method is to acquire more samples of the scene so as to get some additional information which can be utilized, while merging the samples to get a high resolution image. These samples can be acquired by sub-pixel shifts of the camera, by changing scene illumination or by changing the focus of the camera.

Tsai and Huang [1] were the first to propose a frequency domain approach to reconstruction of a high resolution image from a sequence of undersampled low resolution, noise-free images. Ur and Gross use the Papoulis-Brown generalized sampling theorem to obtain an improved resolution picture from an ensemble of spatially shifted pictures [12]. However, these shifts are assumed to be known by the authors. An iterative

backpropagation method is used in [2], wherein a guess of the high resolution output image is updated according to the error between the observed and the low resolution images obtained by simulating the imaging process. But back-propagation methods can be used only for those blurring processes for which such an operator can be calculated. Shekarforoush et al. [3] use MRFs to model the images and obtain 3D high resolution visual information (albedo and depth) from a sequence of displaced low resolution images. The effect of sampling a scene at a higher rate is acquired by having interframe sub-pixel displacements. But they do not consider the case of blurred observations. Elad and Feuer [13] propose a unified methodology for super-resolution restoration from several geometrically warped, blurred, noisy and downsampled measured images by combining ML, MAP and POCS approaches. Chiang and Boult [14] use edge models and a local blur estimate to develop an edge-based super-resolution algorithm. Recently Rajan and Chaudhuri proposed a generalized interpolation scheme and used it to generate super-resolution images from photometric stereo [15]. Here we present a new technique wherein a sequence of low resolution spatially varying blurred and noisy observations is used to simultaneously estimate the super-resolved depth and the image of a scene. Both the high resolution blur and focused image are modeled as separate Markov Random Fields (MRFs). The maximum *a posteriori* estimates of depth and the focused image of the scene are recovered using the simulated annealing algorithm.

4 Low resolution image and blur formation

We briefly present the formation of a low resolution image and blur from their respective high resolution counterparts. Note that the problem we solve here is actually the inverse. Suppose the low resolution image sensor plane is divided into $M_1 \times M_2$ square sensor elements and $\{y_{i,j}\}$, $i = 0, \ldots, M_1 - 1$ and $j = 0, \ldots, M_2 - 1$ are the low resolution intensity values. For a decimation ratio of q, the high resolution grid will be of size $qM_1 \times qM_2$ and $\{z_{k,l}\}$, $k = 0, \ldots, qM_1 - 1$ and $l = 0, \ldots, qM_2 - 1$ will be the high resolution intensity values. The forward process of obtaining $\{y_{i,j}\}$ from $\{z_{k,l}\}$ is written as [16]

$$y_{i,j} = \frac{1}{q^2} \sum_{k=qi}^{(q+1)i-1} \sum_{l=qj}^{(q+1)j-1} z_{k,l} \qquad (3)$$

i.e., the low resolution intensity is the average of the high resolution intensities over a neighborhood of q^2 pixels.

We assume that the space-varying blur (PSF) is Gaussian in nature. Figure 1 illustrates the formation of the low resolution observations using the low resolution blur kernels that are implicitly embedded in the H matrix. In the figure, $\sigma^H(i,j)$ and $\sigma^L(i,j)$ denote the high and low resolution blurs, respectively, while $z(i,j)$ is the high resolution image. Downsampling by a factor of 2 is denoted by $\downarrow 2$. $g(i,j)$ is the decimated image which is subsequently blurred by the space varying blurring kernel through H to obtain the low resolution observation $y(i,j)$. Noise is uncorrelated between different low resolution images.

5 Super-resolved depth and image recovery using MRF models

The super-resolution problem is cast in a restoration framework. There are p observed images $\{Y_i\}_{i=1}^p$ each of size $M_1 \times M_2$. These images are decimated, blurred and noisy versions of a single high resolution image $\mathbf{z}$ of size $N_1 \times N_2$, where $N_1 = qM_1$ and $N_2 = qM_2$. If $\underline{\mathbf{y_i}}$ is the $M_1M_2 \times 1$ lexicographically ordered vector containing pixels from the low resolution image Y_i, then a vector $\underline{\mathbf{z}}$ of size $q^2M_1M_2 \times 1$ containing pixels of the high resolution image can be formed by placing each of the $q \times q$ pixel neighborhoods sequentially so as to maintain the relationship between a low resolution pixel and its corresponding high resolution pixel. After incorporating the blur matrix and noise vector, the image formation model is written as

$$\underline{\mathbf{y_i}} = H_i \; D \; \underline{\mathbf{z}} + \underline{\mathbf{n_i}}, \quad i = 1, \ldots, p \qquad (4)$$

where D is the decimation matrix of size $M_1M_2 \times q^2M_1M_2$, H_i's are the low resolution space varying blurring matrix (PSF) of size $M_1M_2 \times M_1M_2$ with blurring parameters given by $\sigma_i^L(k,l)$, $\underline{\mathbf{n_i}}$ is the $M_1M_2 \times 1$ noise vector and p is the number of low resolution observations. The decimation matrix D consists of q^2 values of $\frac{1}{q^2}$ in each row and has the form [16]

$$D = \frac{1}{q^2} \begin{bmatrix} 1\,1\ldots1 & & & 0 \\ & 1\,1\ldots1 & & \\ & & \ddots & \\ 0 & & & 1\,1\ldots1 \end{bmatrix} \qquad (5)$$

Our problem now reduces to estimating $\underline{\mathbf{z}}$ and the blur parameters σ_{k,l_i}'s given $\underline{\mathbf{y_i}}$'s, which is clearly an ill-posed problem. Once the blurs are determined it is straight forward to obtain the depth map.

We model the both the high resolution image as well as the blurs as separate Markov Random Fields. Let S and Z denote the random fields corresponding to the high-resolution space-variant blur parameter $s_{k,l}(= \sigma^H(k,l))$ and high-resolution focused image

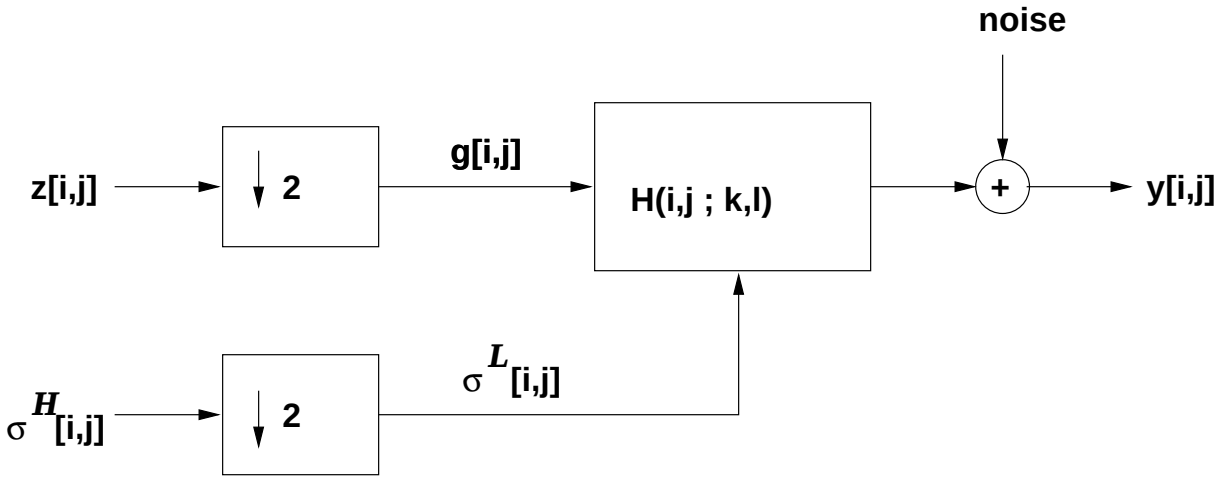

Figure 1: Low resolution image formation from high resolution image and blur.

over the $N_1 \times N_2$ lattice of sites $\mathcal{L}$, respectively. We assume that S can take B possible levels and Z can take C possible levels. The *a posteriori* conditional joint probability of S and Z is given by $P[S = s, Z = z|Y_1 = y_1, \ldots, Y_p = y_p]$. From Bayes' rule,

$$P[S = s, Z = z|Y_1 = y_1, \ldots, Y_p = y_p] = \frac{P[Y_1 = y_1, \ldots, Y_p = y_p|S = s, Z = z]P[S = s, Z = z]}{P[Y_1 = y_1, \ldots, Y_p = y_p]}. \quad (6)$$

The random fields S and Z can be assumed to be statistically independent. Since the denominator in equation (6) is not a function of s or z, the maximum *a posteriori* (MAP) problem of simultaneous estimation of high resolution space-variant blur identification and super-resolved image can be posed as:

$$\max_{s,z} P[Y_1 = y_1, \ldots, Y_p = y_p|S = s, Z = z] \times P[S = s] \times P[Z = z]. \quad (7)$$

Note that the random fields S and Z are high resolution while the observations are low resolution. Taking the log of posterior probability, and since $\underline{\mathbf{n}}_i$'s are independent, equation (7) can be rewritten as

$$\max_{s,z} \sum_{i=1}^{p} \log P[Y_i|S = s, Z = z] + \log P[S = s] + \log P[Z = z]. \quad (8)$$

Since noise is assumed to be i.i.d. Gaussian,

$$\sum_{i=1}^{p} P[Y_i = y_i|S = s, Z = z] = \sum_{i=1}^{p} \log \frac{1}{(2\pi\sigma_\eta^2)^{\frac{M_1 M_2}{2}}} \exp\left\{-\frac{\| \underline{\mathbf{y}}_i - H_i D\underline{\mathbf{z}} \|^2}{2\sigma_\eta^2}\right\} = -\sum_{i=1}^{p} \frac{\| \underline{\mathbf{y}}_i - H_i D\underline{\mathbf{z}} \|^2}{2\sigma_\eta^2} - \frac{M_1 M_2}{2} \log(2\pi\sigma_\eta^2), \quad (9)$$

where σ_η is the noise variance.

Since S and Z are both modeled as MRFs, the priors $P[S = s]$ and $P[Z = z]$ have a Gibbs distribution given by

$$P[S = s] = \frac{1}{K^s} exp\{-\sum_{c \in \mathcal{C}} V_c^s(s)\}$$

and

$$P[Z = z] = \frac{1}{K^z} exp\{-\sum_{c \in \mathcal{C}} V_c^z(z)\}$$

where K^s and K^z are normalizing constants known as partition functionss , $V_c(.)$ is the clique potential and $\mathcal{C}$ is the set of all cliques. Thus the posterior energy function to be maximized is

$$-\sum_{i=1}^{p} \frac{\| \underline{\mathbf{y}}_i - H_i D\underline{\mathbf{z}} \|^2}{2\sigma_\eta^2} - \sum_{c \in \mathcal{C}} V_c^s(s) - \sum_{c \in \mathcal{C}} V_c^z(z) \quad (10)$$

which is equivalent to minimizing

$$\sum_{i=1}^{p} \frac{\| \underline{\mathbf{y}}_i - H_i D\underline{\mathbf{z}} \|^2}{2\sigma_\eta^2} + \sum_{c \in \mathcal{C}} V_c^s(s) + \sum_{c \in \mathcal{C}} V_c^z(z) \quad (11)$$

Smoothness is an assumption underlying a wide range of physical phenomena. However, careless imposition of the smoothness criterion can result in undesirable, oversmoothed solutions. This could happen at points

of discontinuities either in the image or in the depth map. Hence it is necessary to take care of discontinuities. Smoothness constraints on the estimates of the space-variant blur parameter and the intensity process are encoded in the potential function. Preservation of disconitnuities are done through line fields [17]. The horizontal and vertical line fields corresponding to the blurring process are denoted by $l^s_{i,j}$ and $v^s_{i,j}$, respectively, while the line fields corresponding to the intensity process are denoted by $l^z_{i,j}$ and $v^z_{i,j}$. Simulated Annealing (SA) is used to obtain the MAP estimates of the space-variant blur and the super-resolved image simultaneously. Since the random fields S and Z are assumed to be statistically independent, the values of $s_{i,j}$ and $z_{i,j}$ are changed in the SA alogirthm independently of each other. The posterior energy function to be minimized is now defined as

$$\sum_{i=1}^{p} \frac{\| \underline{\mathbf{y}}_i - H_i D \underline{\mathbf{z}} \|^2}{2\sigma_\eta^2} + E_s + E_z \qquad (12)$$

where

$$\begin{aligned} E_s = \; & \textstyle\sum_{i,j} \mu_s [(s_{i,j} - s_{i,j-1})^2 (1 - v^s_{i,j}) \\ + \; & (s_{i,j+1} - s_{i,j})^2 (1 - v^s_{i,j+1}) \\ + \; & (s_{i,j} - s_{i-1,j})^2 (1 - l^s_{i,j}) \\ + \; & (s_{i+1,j} - s_{i,j})^2 (1 - l^s_{i+1,j})] \\ + \; & \gamma_s [l^s_{i,j} + l^s_{i+1,j} + v^s_{i,j} + v^s_{i,j+1}] \end{aligned}$$

and

$$\begin{aligned} E_z = \; & \textstyle\sum_{i,j} \mu_z [(z_{i,j} - z_{i,j-1})^2 (1 - v^z_{i,j}) \\ + \; & (z_{i,j+1} - z_{i,j})^2 (1 - v^z_{i,j+1}) \\ + \; & (z_{i,j} - z_{i-1,j})^2 (1 - l^z_{i,j}) \\ + \; & (z_{i+1,j} - z_{i,j})^2 (1 - l^z_{i+1,j})] \\ + \; & \gamma_z [l^z_{i,j} + l^z_{i+1,j} + v^z_{i,j} + v^z_{i,j+1}]. \end{aligned}$$

Parameters μ and γ correspond to the relative weights of the smoothness term and the penalty term necessary to prevent occurance of spurious discontinuities.

6 Experimental Results

We present some results on the proposed technique to recover super-resolved depth and image from defocused images. Figure 2 shows two of the five low resolution images used in our simulations. The defocused Taj images were generated such that the low-resolution blurs $\sigma^L_{i+1}(k,l) = 0.5 \times \sigma^L_i(k,l), \quad i = 1, \ldots, 4$. As mentioned earlier, such a linear relationsip exists between the blurs when defocused images of a scene are obtained using different values of the camera aperture. Note that $\sigma^L_1(k,l)$ is the decimated

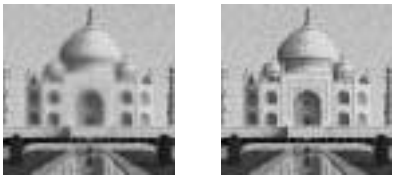

Figure 2: Two of the low resolution observations of the Taj image.

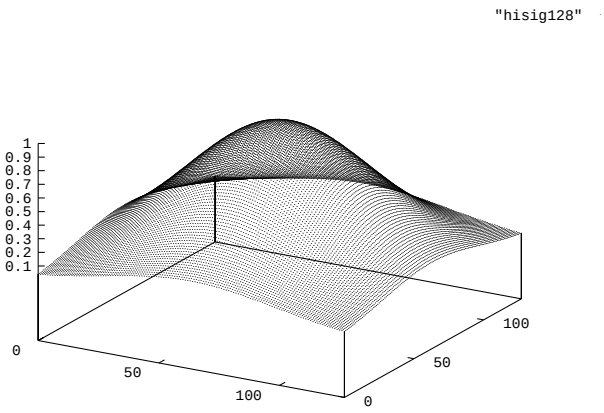

Figure 3: The true high resolution blur whose decimation yields the first low resolution blur.

version of the true high resolution blur which is generated using $\sigma^H(k,l) = a \;\exp(-\frac{(k-\frac{N}{2})^2+(l-\frac{N}{2})^2}{2b^2})$ and plotted in Figure 3. In our experiment, the values are $N = 64$, $a = 1.0$, and $b = 35.0$. We have chosen a decimation factor of 2. The original Taj image is decimated and blurred using the space-varying Gaussian blurring kernels formed from the low resolution blurs. The zero-order hold expansion of the Taj image is shown in Figure 4.

The initial estimate chosen for the high resolution blur was the output obtained using the complex spectrogram, as described in [10]. A square window of size 16×16 was used for the purpose. The bilinear interpolation of the least blurred image was chosen as the initial estimate for the true focused image. The estimated values of the super-resolved blur parameter and the super-resolved image are shown in Figure 5 (a) and Figure 5 (b), respectively. We can see the blockiness caused due to the pixel replication technique of image expansion is absent in the super-resolved image. Next, we consider the case where the blurring is constant over a certain contiguous region of the image and then

Figure 4: The zero-order hold expansion of the Taj image.

varies linearly over a second region and finally is constant again over the remaining part of the image. Two such blurred images of the Sail image are shown in Figure 6(a) and (b). The depth profile is shown in Figure 7 where the constant blur regions are of widths 32 pixels each. The estimated super-resolved blur parameters are shown in Figure 8(a) and the super-resolved image in Figure 8(b).The super-resolved image recovery technique described has performed quite well. The figures on the sail as well as the thin lines on the sail are discernible.

7 Conclusions

We have presented a technique to simultaneously generate a super-resolved depth map and image from a sequence of low resolution space varying blurred observations. Both the high resolution blur and the image are modeled individually as MRFs and a MAP estimate is used. The depth at a point in the scene can be calculated from the estimated blur at that point through the depth from defocus formulation. In the method described in this paper, we recover both depth and the true image at a higher resolution than any of the observations. Future work will involve fine tuning the parameters of the final cost function for further improvement in the results, as well as using other models, like the Ising model, for the prior probabilities of the blur and the intensity fields.

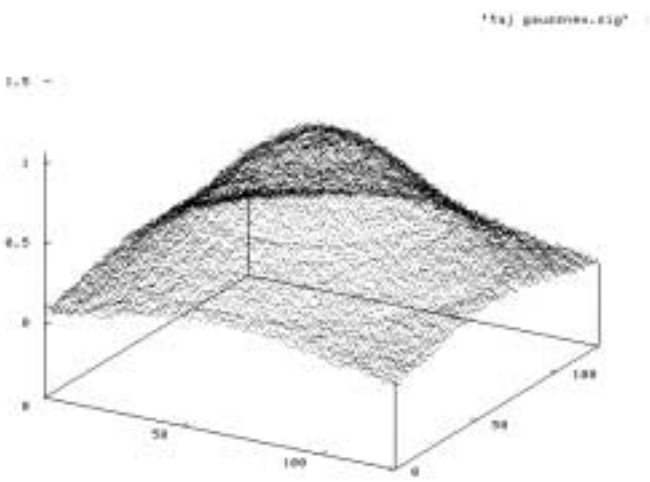

(a)

(b)

Figure 5: (a) The estimated high resolution blur and (b) the recovered super-resolved Taj image.

References

[1] R. Y. Tsai and T. S. Huang, "Multiframe image restoration and registration," in *Advances in Computer Vision and Image Processsing*, pp. 317–339, JAI Press Inc., 1984.

[2] M. Irani and S. Peleg, "Improving resolution by image registration," *CVGIP:Graphical Models and Image Processing*, vol. 53, pp. 231–239, March 1991.

[3] Hassan Shekarforoush, Marc Berthod, Josiane Zerubia and M. Werman, "Sub-pixel bayesian estimation of albedo and height," *International Journal of Computer Vision*, vol. 19, no. 3, pp. 289–300, 1996.

[4] R. R. Schultz and R. L. Stevenson, "Extraction of high-resolution frames from video sequences," *IEEE Trans. on Image Processing*, vol. 5, pp. 996–1011, June 1996.

[5] A. P. Pentland, "Depth of scene from depth of field," in *Proc. of Image Understanding Work-*

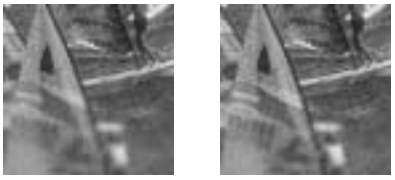

Figure 6: Two of the low resolution observations of the Sail image.

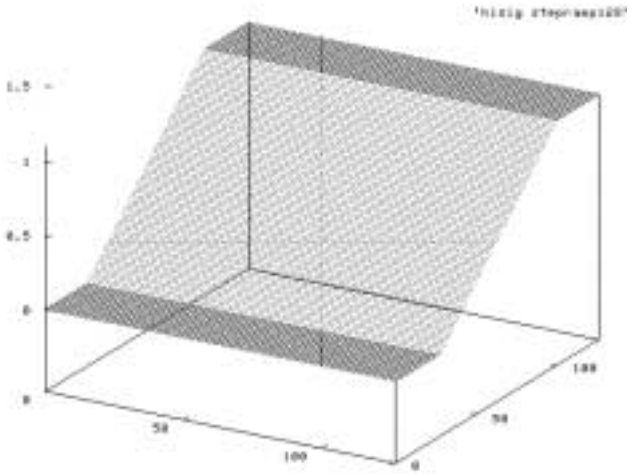

Figure 7: The true high resolution blur whose decimation yields the first low resolution blur.

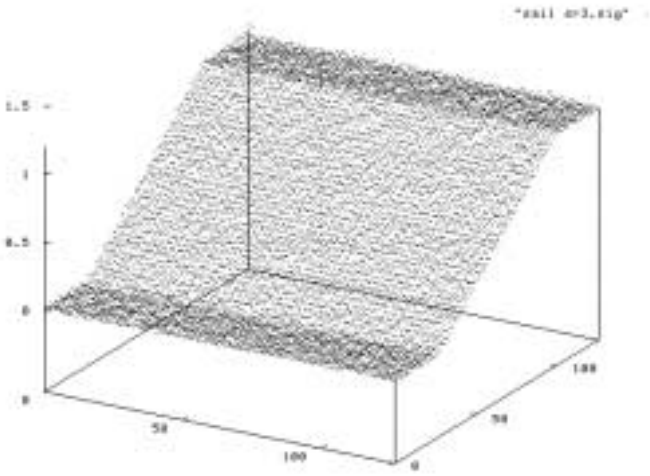

(a)

(b)

Figure 8: (a) The estimated high resolution blur and (b) the recovered super-resolved Sail image.

shop, (Palo Alto, USA), pp. 253–259, 1982.

[6] A. P. Pentland, "A new sense for depth of field," *IEEE Trans. on Pattern Anal. and Machine Intell.*, vol. 9, pp. 523–531, July 1987.

[7] M. Subbarao, "Parallel depth recovery by changing camera parameters," in *Proc. of IEEE CVPR*, (Florida, USA), pp. 149–155, 1988.

[8] S. Chaudhuri and A. N. Rajagopalan, *Depth from defocused images : A real aperture imaging approach*. Springer-Verlag, New York, 1999.

[9] A. N. Rajagopalan and S. Chaudhuri, "Space-variant approaches to recovery of depth from defocused images," *Computer Vision and Image Understanding*, vol. 68, pp. 309–329, Dec. 1997.

[10] A. N. Rajagopalan and S. Chaudhuri, "A variational approach to recovering depth from defocused images," *IEEE Trans. on Pattern Analysis and Machine Intelligence*, vol. 19, pp. 1158–1165, Oct. 1997.

[11] A. N. Rajagopalan and S. Chaudhuri, "An MRF model based approach to simultaneous recovery of depth and restoration from defocused images," *IEEE Trans. on Pattern Analysis and Machine Intelligence*, vol. 21, pp. 577–589, July 1999.

[12] H. Ur and D. Gross, "Improved resolution from sub-pixel shifted pictures," *CVGIP:Graphical Models and Image Processing*, vol. 54, pp. 181–186, March 1992.

[13] M. Elad and A. Feuer, "Restoration of a single super-resolution image from several blurred,

noisy and undersampled measured images," *IEEE Trans. on Image Processing*, vol. 6, pp. 1646–1658, December 1997.

[14] M.-C. Chiang and T. E. Boult, "Local blur estimation and super-resolution," in *Proc. CVPR, Puerto Rico, USA*, pp. 821–826, 1997.

[15] D. Rajan and S. Chaudhuri, "A generalized interpolation scheme for image scaling and super-resolution," in *Proc. of Erlangen Workshop '99 on Vision, Modelling and Visualization, University of Erlangen-Nuremberg*, (Germany), pp. 301–308, Nov. 1999.

[16] R. R. Schultz and R. L. Stevenson, "A Bayesian approach to image expansion for improved definition," *IEEE Trans. on Image Processing*, vol. 3, pp. 233–242, May 1994.

[17] S. Geman and D. Geman, "Stochastic relaxation, Gibbs distribution and the Bayesian restoration of image," *IEEE Trans. on Pattern Analysis and Machine Intelligence*, vol. 6, no. 6, pp. 721–741, 1984.